Extreme Mechanics Letters 59 (2023) 101952

Contents lists available at ScienceDirect

Extreme Mechanics Letters

journal homepage: www.elsevier.com/locate/eml

Exceptionally strong boron nitride nanotube aluminum composite interfaces

Yingchun Jiang [a,1], Ning Li [b,1], Zihan Liu [a], Chenglin Yi [a], Huimin Zhou [c], Cheol Park [d], Catharine C. Fay [d], Jia Deng [c], Huck Beng Chew [b], Changhong Ke [a,e,*]

[a] Department of Mechanical Engineering, State University of New York at Binghamton, Binghamton, NY 13902, USA
[b] Department of Aerospace Engineering, University of Illinois at Urbana-Champaign, Urbana, IL 61801, USA
[c] Department of Systems Science and Industrial Engineering, State University of New York at Binghamton, Binghamton, NY 13902, USA
[d] Advanced Materials and Processing Branch, NASA Langley Research Center, Hampton, VA 23681, USA
[e] Materials Science and Engineering Program, State University of New York at Binghamton, Binghamton, NY 13902, USA

ARTICLE INFO

Article history:
Received 24 October 2022
Received in revised form 30 November 2022
Accepted 21 December 2022
Available online 28 December 2022

Keywords:
Boron nitride nanotube
Metal matrix composite
Interfacial shear
Oxidation
Single-nanotube pullout experiments

ABSTRACT

We report the direct strength property measurements along boron nitride nanotube (BNNT) aluminum (Al) composite interface using *in situ* scanning electron microscopy single-nanotube pullout techniques. The nanomechanical measurements reveal that the BNNT-Al interface possesses an average interfacial shear strength of ~46 MPa and a maximum shear load of ~340 nN, and is over 60% stronger than the comparable carbon nanotube (CNT) -Al interface. This strong interface enables significant loading of the nanotube during pull-out from the metal matrix with a generated maximum tensile stress close to its intrinsic strength limit. Density functional theory (DFT) calculations reveal stronger interfacial physio- and chemisorption interactions on an oxidized Al interface with hexagonal boron nitride (hBN) as compared to graphene, which are in contrast to comparable binding properties of hBN and graphene with pure Al. The exceptional Al-BNNT strength properties can thus be attributed to a partially oxidized metal-nanotube binding interface, which has important implications for optimizing the local interfacial load transfer and bulk properties of BNNT-metal nanocomposites.

1. Introduction

Low-dimensional hexagonal boron nitride (hBN) and graphene are promising and competing fillers for reinforcing a wide variety of polymeric, metallic, and ceramic materials, which are attributed to their low density and high surface-to-volume characteristics, as well as their extraordinary material properties. The covalent and partially ionic B–N bonds in boron nitride nanotubes (BNNTs) not only lead to an ultra-high Young's modulus of up to 1.3 TPa and tensile strength of ~33 GPa (measured; ~90 GPa theoretical) [1–13], both of which are comparable to those of purely covalent-bonded carbon nanotubes (CNTs), but also results in corrugated electronic structures with high binding affinity as compared to the isotropic and electrically neutral surface of graphene or CNT. BNNT reportedly binds more strongly to polymers than CNT, thanks to the Coulomb interactions on the BN-polymer interface [14]. Recent studies reveal that the hBN-ceramic interface bears larger shear than the comparable interface formed with graphene or CNT, which is attributed to the higher sliding energy barrier of rugged anisotropic energy landscape surfaces (for hBN) as compared to smooth isotropic energy surfaces (for graphene/CNT) [15]. These findings, based on direct nanomechanical measurements and atomistic simulations, provide scientific foundations for understanding the interfacial shear and hBN strengthening mechanism in polymers and ceramics. Comparatively, our understanding of the adhesion and shear strength properties along the hBN-metal interface remains elusive.

From the viewpoint of metal-based nanocomposites, BNNT possesses distinct advantages over CNT as the preferred reinforcing filler due to its superior thermal inertness and chemical stability. BNNT is a large-bandgap insulator and starts to oxidize at >900 °C versus ~450 °C for CNT which is either metallic or semiconductive. The addition of BNNTs to metals does not cause corrosion and is less prone to the formation of metallic carbides, which are major challenges for CNT-reinforced metal composites [16]. Substantial mechanical property enhancement of BNNT-metal composites has been documented in the literature [17–20], including a 9-fold increase in the tensile strength of an aluminum (Al)-coated single BNNT composite [17], and

* Corresponding author at: Department of Mechanical Engineering, State University of New York at Binghamton, Binghamton, NY 13902, USA.
E-mail addresses: hbchew@illinois.edu (H.B. Chew), cke@binghamton.edu (C. Ke).
[1] Authors contributed equally.

https://doi.org/10.1016/j.eml.2022.101952
2352-4316/

a 50% increase in the tensile and compressive yield strength for an Al composite with a 5 vol.% of BNNTs [18]. While these advances qualitatively demonstrate the effective load transfer along a BNNT-metal interface, a quantitative understanding of the fundamental reinforcing mechanism remains unexplored.

Here, we report the first direct and quantitative measurements of the mechanical strength along the BNNT-aluminum composite interface using *in situ* scanning electron microscopy (SEM) nanomechanical single-nanotube pullout techniques along with companion density function theory (DFT) calculations. The single-nanotube pullout measurements reveal that the BNNT-Al interface possesses an interfacial shear strength of ∼46 MPa and is over 60% stronger than the comparable CNT-Al interface. DFT calculations of hBN and graphene interactions with Al reveal the interfacial physio- and chemisorption interaction, as well as the strengthening effect of the oxide layer in the partially-oxidized metal matrix. The superior load transfer properties along the BNNT-metal interface help elucidate the reinforcing mechanism of BNNTs as extraordinary filler materials for light, strong and durable metal matrix composites.

2. Results and discussion

The single-nanotube pullout technique, illustrated in Fig. 1a, employs a pre-calibrated atomic force microscopy (AFM) cantilever as a force sensor to stretch out a protruding single nanotube that is partially sandwiched between two layers of metal films fabricated by electron beam deposition (Fig. 1b; see *Experimental Methods* and Fig. S5 in the Supplementary Materials). This work employs BNNTs which are produced using high-temperature pressure (HTP) methods [21]. Such nanotubes are reported to have high crystallinity, and are mostly double-walled with a median diameter of 2.9 nm [22]. Electron beam induced deposition (EBID) of platinum (Pt) was used to enhance the attachment of the protruding nanotube with the probe tip of the AFM sensor. The electron microscopy inspection (Fig. S4 and Fig. S5) shows that the protruding nanotube and the pulled-out nanotube have clean surfaces that are free of any noticeable matrix residual. Therefore, the observed nanotube pullout occurs as a result of a fracture of the nanotube-matrix interface. In addition to the successful pullout of nanotubes, we observe nanotube fracture and telescopic pullout events during our nanomechanical measurements (Fig. 1c). Fig. 1d shows the dependence of the measured pullout force on the embedded nanotube length based on 20 different successful nanotube pullout experiments (red dots), which displays a similar shear-lag behavior as observed in the prior single-nanotube pullout studies of BNNT-polymer and BNNT-ceramic interfaces [14,23]. The pullout force increases proportionately with the embedded nanotube length, and reaches a saturation at ∼339 ± 49 nN. Achieving this remarkable load transfer along the nanotube-metal interface requires (a) strong nanotube-metal binding interaction, along with (b) ultra-high breaking strength of the nanotube. Specifically, the measured plateaued pullout force of ∼339 nN translates to a maximum nominal tensile stress of ∼62 GPa in the protruded BNNT based on the entire cross-section area of the nanotube calculated using its median diameter. The result implies that the tensile strength of the employed BNNTs is substantially higher than the experimentally measured value of ∼33 GPa [10] reported on BNNTs produced using chemical vapor deposition (CVD) methods, but remains well below the theoretical intrinsic strength limit of ∼90 GP that corresponds to a maximum applied tensile strain of ∼10% [11–13]. We remark that our estimated nominal tensile stress in the nanotube neglects the effect of the Pt coating on the protruding nanotube and cannot account for the uncertainty associated with the nanotube geometry (i.e., the number of tube shells and the tube diameter, which are beyond the resolution limit of the electron beam). The substantial loading of the nanotube during pullout is also indicated by the observed nanotube fracture and telescopic pullout events, as exemplified in Fig. 1c. In this particular event, the applied stretching force reaches ∼296 nN, corresponding to a maximum nominal tensile strength of ∼54 GPa in the fractured BNNT, while the embedded nanotube-metal interface remains intact.

Fig. 1d also displays our prior nanotube pullout data on comparable CNT-Al interface by using the same sample preparation and nanomechanical pullout scheme (black dots) [24]. The pullout force curve obtained for CNT-Al interfaces shows a similar bilinear shear-lag trend with a plateau force of ∼217 nN. It is noted that the median diameter of the employed BNNTs (2.9 nm) is ∼6.5% smaller than that of the employed CNTs (3.1 nm). The ∼56.2% larger plateau force measured for the BNNT-Al interface as compared to the CNT-Al interface translates to a remarkable ∼66.8% higher interfacial shear load carrying capacity on a per unit area basis. The interfacial strength of the nanotube-metal interface is also indicated by the average IFSS, which is calculated as the ratio of the pullout force and the embedded nanotube surface area based on the data points in the initial increasing segment of the pullout force curve. We obtain an average interfacial shear strength (IFSS) of ∼46.0 ± 6.5 MPa for the BNNT-Al interface, which is, on average, ∼60.3% higher than that of the CNT-Al interface (∼28.7 ± 3.4 MPa) based on the nanotubes' median diameters. Our measured IFSS for BNNT-Al is compared even more favorably with the CNT-Al value (∼24.8 MPa) reported by Kawasaki et al. [25], and is consistent with an interfacial strength in the order of ∼50 MPa inferred from the tensile measurement of BNNT-Al hybrids [26].

While studies have reported the formation of reaction products such as AlB and AlN across the BNNT-Al interface at high temperatures of 650 °C [27], such reaction products, which may be rampant in bulk nanotube-metal composites fabricated by powder metallurgy and casting, are likely absent along the nanotube-metal interface characterized here in view of the much lower temperatures (∼100 °C or below) used in the fabrication of our sandwiched structure. Nevertheless, it is noted that because Al is an active metal, a ∼2 nm thick metal oxide layer is partially-formed along the measured BNNT-Al and CNT-Al interfaces as a result of oxygen and moisture-induced metal passivation during the sample preparation process at ambient environment [24,28] (Fig. 1a insert, see Fig.S6 and *Experimental Methods* in the Supplementary Materials). Therefore, it is essential to take into account the nanotube-aluminum oxide (Al_2O_3) interaction in the understanding of the BNNT-Al and CNT-Al interfacial measurements. In this regard, we conduct plane-wave density functional theory (DFT) calculations using Vienna Ab-initio Simulation Package (VASP) [29–31] to elucidate the interfacial interactions between Al and BNNT or CNT. We account for the effects of metal passivation by considering four separate model structures in our DFT supercells: (a) Al-hBN, (b) Al-graphene, (c) Al_2O_3-hBN, and (d) Al_2O_3-graphene. The respective interfaces in each of these supercells comprise of a 1 × 1 unit cell of Al(111) or O-terminated Al_2O_3(0001) placed on top of a 2 × 2 unit cell of monolayer graphene or hBN, which results in average mismatch strains of 1.0% (Al-hBN), 0.7% (Al-graphene), 4.5% (Al_2O_3-hBN), and 2.7% (Al_2O_3-graphene). Periodic boundary conditions are imposed in all directions, and a 10 Å vacuum layer is introduced at the top of each supercell to prevent the interaction between periodic images in the vertical direction (x_3-direction). The interaction between electrons and ions is described by the Perdew–Burke–Ernzerhof (PBE) functional and the projector augmented wave (PAW) based pseudopotentials with van der Waals force corrections calculated by the DFT-D2 method of Grimme for exchange

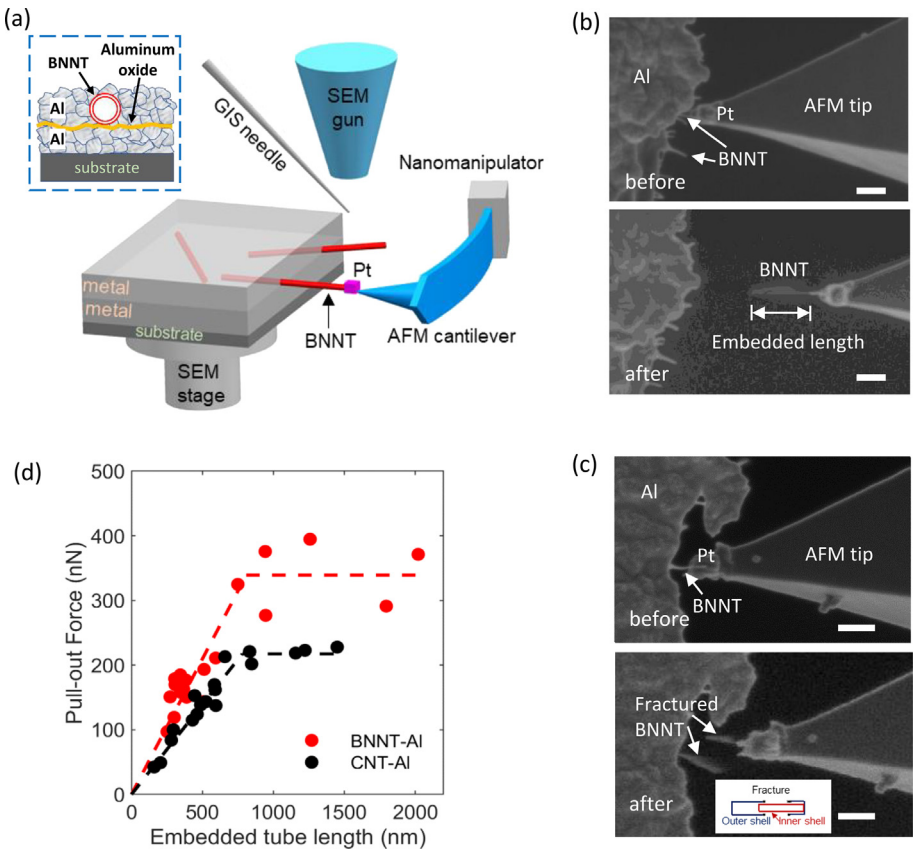

Fig. 1. (a) Schematic of in situ SEM single-nanotube pullout technique. The upper left drawing illustrates the cross-section of the engineered nanotube-metal interface. (b) Selected SEM snapshots of a successful single BNNT pullout from the Al matrix. (c) Selected SEM snapshots of a nanotube fracture and telescopic pullout; the insert drawing illustrates the telescopic pullout of the inner tube shell from the fractured outer shell for a double-walled BNNT. (d) The comparison of the measured pullout force for both BNNT-Al and CNT-Al interfaces (the data for CNT-Al interfaces are reproduced from Ref. [24]). The dashed lines are the respective bilinear fitting curves. The scale bars in (b) and (c) are all 500 nm. All drawings are not to scale.

and correlation. A gamma-centered Monkhorst–Pack k-points of $6 \times 6 \times 1$ is specified to sample the Brillouin zone in our calculations. The top three rows of atoms (Al or O) are fixed in space to represent a bulk crystal structure, while we relax the remaining structure with a cutoff energy of 550 eV, and adopt a criterion of $1e^{-10}$ eV as the energy cut-off for convergence.

Fig. 2 shows the fully-relaxed atomistic configurations for all four model structures, along with contours of the electron localized function (ELF) along a cross-sectional cut in the vertical direction. The ELF contours, ranging from 0 to 1, denote the likelihood of finding an electron near another electron with the same spin. We observe low ELF values across both Al-hBN and Al-graphene interfaces, which suggest weak physisorption across both these interfaces and are consistent with the literature [26,32,33]. Despite similar weak interfacial interactions for hBN and graphene with pure Al, the interfacial properties are dramatically different for hBN and graphene with an oxidized interface, i.e. Al_2O_3. In the case of Al_2O_3-graphene, localized electron pockets reside near the O-terminated interface, due to the polarizing effects of the electronegative O atoms interacting with the orbitals of graphene C atoms across the interface [34]. As a result, stronger polar-covalent bonds are now formed across the Al_2O_3-graphene interface – a cross between physisorption and chemisorption – causing an 18% reduction in the interfacial separation distance to ∼2.7 Å versus ∼3.3 Å for Al-graphene. The interfacial interactions are even stronger for Al_2O_3-hBN, with the formation of distinct and directional B–O and N–O covalent bonds across the interface. The single N–O bond within our supercell has a bond length of 1.5 Å, which is within the range of reported N–O bond lengths of 1.39–1.61 Å in a tetrahedral configuration [35]. The two B–O bonds within our supercell have bond lengths of 1.52 Å and 1.58 Å, respectively, which are also close to previously reported tetrahedral B–O bond length of 1.45–1.47 Å [36,37]. The presence of these B–O and N–O bonds cause slight stretching of neighboring B–N bonds, resulting in bond lengths of up to 1.60 Å from the equilibrium bond length of 1.45 Å in hBN. All N–B–O and N–B–N bond angles are within 10° of the 109.5° bond angles for tetrahedron structures. These results confirm the formation of sp^3 bonds across the Al_2O_3-hBN interface.

The dramatic change to the interfacial bonding with oxidation is reflected in the adhesion energies for these respective structures calculated by DFT — we rigidly separate the relaxed configuration of each substrate and atomic sheet by 10 Å, and subtract the total energy of the isolated substrate and sheet from the combined structure. We obtain low adhesion energies of 0.76 and 1.19 eV/nm^2 for Al-graphene and Al-hBN, respectively. With an oxidized interface, however, the adhesion energy increases by 7- and 11-folds, to 5.3 and 13.5 eV/nm^2 for Al_2O_3-graphene and Al_2O_3-hBN, respectively. We remark that our adhesion energies for Al-graphene and Al_2O_3-graphene are ∼30% higher than the reported values of 0.57 and 3.68 eV/nm^2 using the Ceperley-Alder form of the local density approximation (LDA) [38], due to consideration of London dispersion effects with DFT-D2.

Since the exposed surfaces/interfaces of the Al matrix are partially oxidized from metal passivation, the interfacial strength properties can be interpreted to span between those for pure Al and O-terminated Al_2O_3. The stronger binding of the atomic sheets with Al_2O_3 versus pure Al, particularly for hBN, reflects the role of surface oxidation in increasing the binding strength across the sheet–substrate interface. Ultimately, this explains the

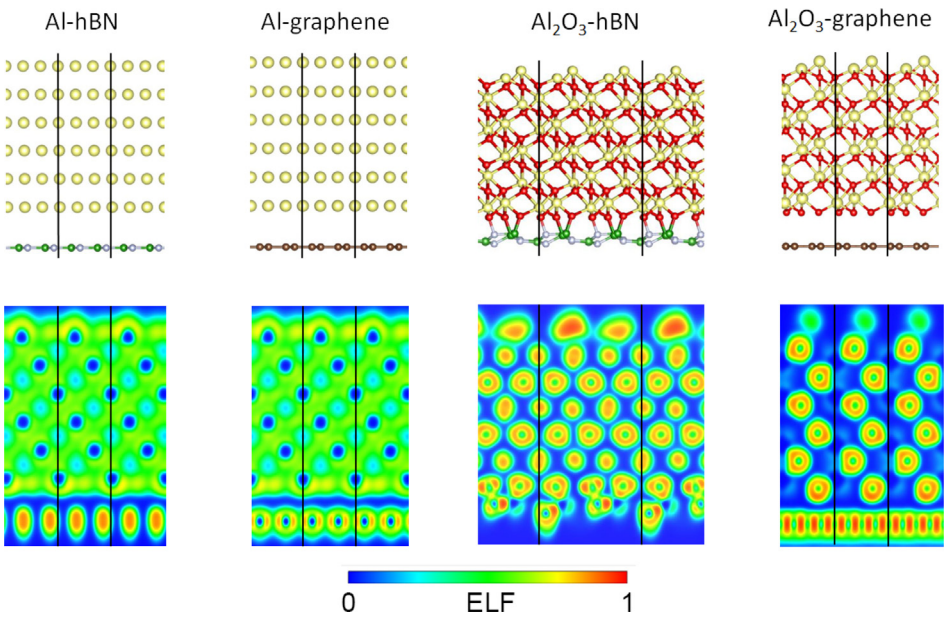

Fig. 2. Side views of the atomistic configurations of Al-hBN, Al-graphene, Al_2O_3-hBN, and Al_2O_3-graphene interface structures, with corresponding electron localized function (ELF). Solid lines denote periodicity of supercells. Atom types are colored: green (B), white (N), brown (C), red (O), pale-yellow (Al).

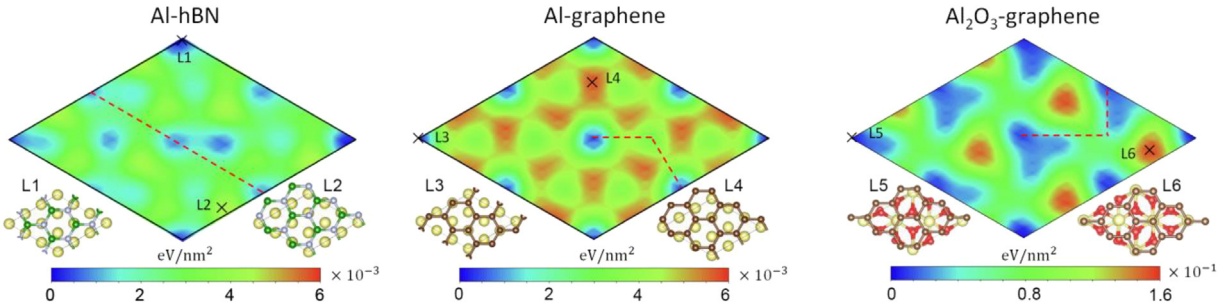

Fig. 3. Sliding energy landscapes for Al-hBN, Al-graphene, and Al_2O_3-graphene interfaces. Red dashed lines denote sampling of minimum energy pathways. Atomistic configurations show bottom-up view of the interfaces at the minimum energy (L1, L3, L5) and maximum barrier energy (L2, L4, L6) locations.

high pullout forces of CNTs and BNNTs from Al matrices (Fig. 1d), resulting in average IFSS of ∼28.7 and ∼46.0 MPa, which are even higher than the ∼19.2 and ∼34.7 MPa interfacial strength reported for silica-CNT and silica-BNNT interfaces [15,23], respectively. The strong Al_2O_3-hBN binding interaction is also consistent with the recently reported bulk property enhancement of BNNT-reinforced Al_2O_3 [39].

The nanomechanical measurements show that the nanotube undertakes substantial tensile stress during pullout from the metal matrix. Our DFT calculations suggest that the pullout of BNNT initiates with the breaking of N–O and B–O (sp^3) bonds formed between the oxidized matrix and the nanotube, and/or the neighboring stretched B–N and O–Al bonds. In the absence of chemisorption along the nanotube-matrix interface, i.e., Al-hBN, Al-graphene, and Al_2O_3-graphene, sliding along the weakly-bonded interfaces becomes the dominant failure mode during nanotube pullout. Fig. 3 shows the potential energy landscapes for interfacial sliding, obtained by iteratively displacing the atomic sheets with respect to the substrate at 20 evenly-spaced intervals along the two in-plane lattice vectors of each supercell. When the pullout force is small, interfacial sliding follows the minimum energy pathways, a sampling of which is shown by dashed red lines in Fig. 3. In contrast, a large pullout force typically induces rapid interfacial sliding along a straight path, and would eventually result in the cross of the peak energy barriers, denoted by L2, L4, and L6 in Fig. 3. Both the minimum and peak energy barriers are slightly higher for Al-graphene than for Al-hBN. Compared to Al-graphene, both the minimum and peak energy barriers are ∼30 times larger for Al_2O_3-graphene, indicating that akin to Al_2O_3-hBN, the formation of the oxide layer is the main contributor to the strong interfacial binding.

Fig. 4 shows that the maximum nominal tensile stress generated in the nanotube during the successful pullout of the BNNT-Al interface is the largest among a variety of CNT or BNNT interfaces formed with metals [24,40,41], ceramics [15,23] and polymers [14,42,43] (see Table S1), and is also closest to the nanotube's theoretical strength limit. The stronger BNNT-metal interface enables a better utilization of the ultra-strong characteristics of the nanotube in the reinforcement of the metal matrix composite. The measured BNNT-Al interface, which is free of any post thermal processing, is stronger than the thermal-annealing enhanced CNT-Al interface (average IFSS ∼35.3 MPa, ∼23% higher than the interface without annealing) [24], and could be further strengthened through increasing the level of metal oxidation in the vicinity of interface via facile thermal processing.

3. Conclusion

In summary, our nanomechanical measurements reveal a much stronger BNNT-Al composite interface than the comparable CNT-Al composite interface as well as CNT or BNNT interfaces with ceramics and polymers. The strong BNNT-metal interface enables

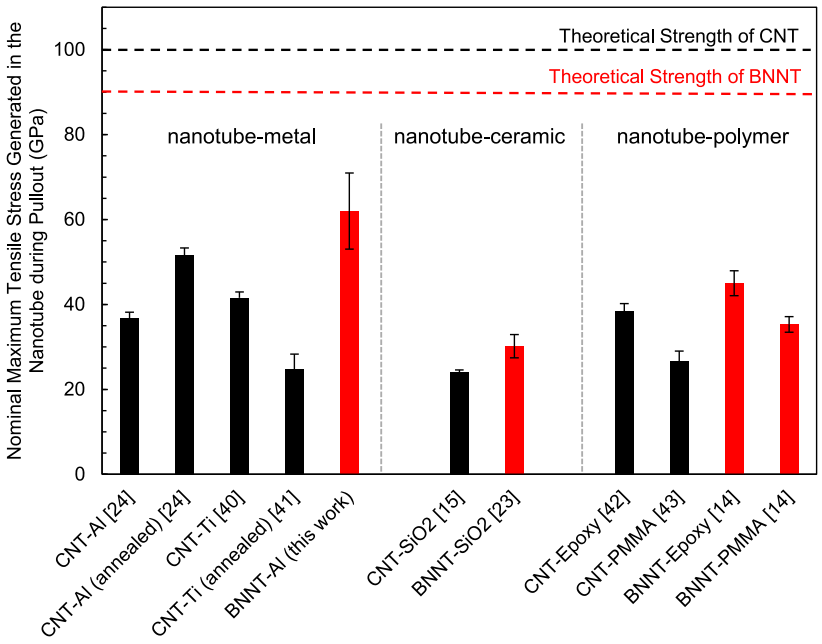

Fig. 4. Comparison of the nominal maximum tensile stress generated in the nanotube during successful pullout based on single-nanotube pullout measurements conducted on a variety of CNT or BNNT interfaces formed with metals, ceramics, and polymers. The employed BNNTs (∼2.9 nm in median diameter) and CNTs (∼3.1 nm in median diameter) in all these nanotube-matrix interface studies are from the same respective sources (i.e., the same types of nanotubes produced using the same synthesis methods). The number in the bracket indicates the reference of the data source.

significant load transfer to strain the embedded nanotubes within the metal matrix to reach tensile loads close to the breaking point, which is optimal for the composite's bulk property enhancement. DFT calculations suggest that the BNNT-metal interface is mechanistically strengthened by the formation of covalent bonds across the partially oxidized metal-nanotube binding interface. The findings of the superior load transfer on the oxidized BNNT-metal interface provides a plausible venue for optimizing the local load transfer and bulk properties of BNNT-metal nanocomposites through interface engineering.

Declaration of competing interest

The authors declare that they have no known competing financial interests or personal relationships that could have appeared to influence the work reported in this paper.

Data availability

Data will be made available on request.

Acknowledgments

The authors acknowledge the support of the National Science Foundation, United States under grant nos. NSF-CMMI 2009134, 2009684, and 2006127, and the United States Air Force Office of Scientific Research under Grant No. FA9550-15-1-0491. The DFT calculations were performed using the computational time provided by the Blue Waters sustained-petascale computing project, which is supported by the Delta research computing project, which is supported by the National Science Foundation (award OCI 2005572), and the State of Illinois. Delta is a joint effort of the University of Illinois at Urbana-Champaign and its National Center for Supercomputing Applications. The use of the Advanced Cyberinfrastructure Coordination Ecosystem: Services & Support (ACCESS), through allocations TG-PHY220010, TG-MAT210010, and TG-MAT210031 is also gratefully acknowledged.

Appendix A. Supplementary data

Supplementary material related to this article can be found online at https://doi.org/10.1016/j.eml.2022.101952.

References

[1] N.G. Chopra, A. Zettl, Measurement of the elastic modulus of a multi-wall boron nitride nanotube, Solid State Commun. 105 (1998) 297–300.
[2] R. Arenal, M.-S. Wang, Z. Xu, A. Loiseau, D. Golberg, Young modulus, mechanical and electrical properties of isolated individual and bundled single-walled boron nitride nanotubes, Nanotechnology 22 (2011) 265704, http://dx.doi.org/10.1088/0957-4484/22/26/265704.
[3] E. Hernandez, C. Goze, P. Bernier, A. Rubio, Elastic properties of C and BxCyNz composite nanotubes, Phys. Rev. Lett. 80 (1998) 4502–4505.
[4] H.M. Ghassemi, C.H. Lee, Y.K. Yap, R.S. Yassar, Real-time fracture detection of individual boron nitride nanotubes in severe cyclic deformation processes, J. Appl. Phys. 108 (2010) 024314, http://dx.doi.org/10.1063/1.3456083.
[5] D.-M. Tang, C.-L. Ren, X. Wei, M.-S. Wang, C. Liu, Y. Bando, D. Golberg, Mechanical properties of bamboo-like boron nitride nanotubes by in situ TEM and MD simulations: strengthening effect of interlocked joint interfaces, ACS Nano. 5 (2011) 7362–7368, http://dx.doi.org/10.1021/nn202283a.
[6] A.P. Suryavanshi, M.-F. Yu, J. Wen, C. Tang, Y. Bando, Elastic modulus and resonance behavior of boron nitride nanotubes, Appl. Phys. Lett. 84 (2004) 2527–2529, http://dx.doi.org/10.1063/1.1691189.
[7] D. Golberg, P.M.F.J. Costa, O. Lourie, M. Mitome, X. Bai, K. Kurashima, C. Zhi, C. Tang, Y. Bando, Direct force measurements and Kinking under elastic deformation of individual multiwalled boron nitride nanotubes, Nano Lett. 7 (2007) 2146–2151, http://dx.doi.org/10.1021/nl070863r.
[8] Y. Zhao, X. Chen, C. Park, C.C. Fay, S. Stupkiewicz, C. Ke, Mechanical deformations of boron nitride nanotubes in crossed junctions, J. Appl. Phys. 115 (2014) 164305, http://dx.doi.org/10.1063/1.4872238.
[9] M. Zheng, X. Chen, C. Park, C.C. Fay, N.M. Pugno, C. Ke, Nanomechanical cutting of boron nitride nanotubes by atomic force microscopy, Nanotechnology 24 (2013) 505719, http://dx.doi.org/10.1088/0957-4484/24/50/505719.
[10] X. Wei, M.-S. Wang, Y. Bando, D. Golberg, Tensile tests on individual multi-walled boron nitride nanotubes, Adv. Mater. 22 (2010) 4895–4899, http://dx.doi.org/10.1002/adma.201001829.
[11] H.F. Bettinger, T. Dumitrică, G.E. Scuseria, B.I. Yakobson, Mechanically induced defects and strength of BN nanotubes, Phys. Rev. B. 65 (2002) 041406, http://dx.doi.org/10.1103/PhysRevB.65.041406.
[12] T. Dumitrica, H.F. Bettinger, G.E. Scuseria, B.I. Yakobson, Thermodynamics of yield in boron nitride nanotubes, Phys. Rev. B. 68 (2003) 085412.

[13] J. Song, H. Jiang, J. Wu, Y. Huang, K.-C. Hwang, Stone–Wales transformation in boron nitride nanotubes, Scr. Mater. 57 (2007) 571–574, http://dx.doi.org/10.1016/j.scriptamat.2007.06.027.
[14] X. Chen, L. Zhang, C. Park, C.C. Fay, X. Wang, C. Ke, Mechanical strength of boron nitride nanotube-polymer interfaces, Appl. Phys. Lett. 107 (2015) 253105, http://dx.doi.org/10.1063/1.4936755.
[15] N. Li, C.M. Dmuchowski, Y. Jiang, C. Yi, F. Gou, J. Deng, C. Ke, H.B. Chew, Sliding energy landscape governs interfacial failure of nanotube-reinforced ceramic nanocomposites, Scr. Mater. 210 (2022) 114413, http://dx.doi.org/10.1016/j.scriptamat.2021.114413.
[16] K.S. Munir, P. Kingshott, C. Wen, Carbon nanotube reinforced titanium metal matrix composites prepared by powder metallurgy—A review, Crit. Rev. Solid State Mater. Sci. 40 (2015) 38–55, http://dx.doi.org/10.1080/10408436.2014.929521.
[17] M. Yamaguchi, D.-M. Tang, C. Zhi, Y. Bando, D. Shtansky, D. Golberg, Synthesis, Structural analysis and in situ transmission electron microscopy mechanical tests on individual aluminum matrix/boron nitride nanotube nanohybrids, Acta Mater. 60 (2012) 6213–6222, http://dx.doi.org/10.1016/j.actamat.2012.07.066.
[18] D. Lahiri, A. Hadjikhani, C. Zhang, T. Xing, L.H. Li, Y. Chen, A. Agarwal, Boron nitride nanotubes reinforced aluminum composites prepared by spark plasma sintering: Microstructure, mechanical properties and deformation behavior, Mater. Sci. Eng. A. 574 (2013) 149–156, http://dx.doi.org/10.1016/j.msea.2013.03.022.
[19] P. Nautiyal, C. Rudolf, A. Loganathan, C. Zhang, B. Boesl, A. Agarwal, Directionally aligned ultra-long boron nitride nanotube induced strengthening of aluminum-based sandwich composite, Adv. Eng. Mater. 18 (2016) 1747–1754, http://dx.doi.org/10.1002/adem.201600212.
[20] M. Antillon, P. Nautiyal, A. Loganathan, B. Boesl, A. Agarwal, Strengthening in boron nitride nanotube reinforced aluminum composites prepared by roll bonding, Adv. Eng. Mater. 20 (2018) 1800122, http://dx.doi.org/10.1002/adem.201800122.
[21] M.W. Smith, K.C. Jordan, C. Park, J.-W. Kim, P.T. Lillehei, R. Crooks, J.S. Harrison, Very long single- and few-walled boron nitride nanotubes via the pressurized vapor/condenser method, Nanotechnology 20 (2009) 505604, http://dx.doi.org/10.1088/0957-4484/20/50/505604.
[22] V. Yamakov, C. Park, J.H. Kang, X. Chen, C. Ke, C. Fay, Piezoelectric and elastic properties of multiwall boron-nitride nanotubes and their fibers: A molecular dynamics study, Comput. Mater. Sci. 135 (2017) 29–42, http://dx.doi.org/10.1016/j.commatsci.2017.03.050.
[23] C. Yi, S. Bagchi, F. Gou, C.M. Dmuchowski, C. Park, C.C. Fay, H.B. Chew, C. Ke, Direct nanomechanical measurements of boron nitride nanotube—ceramic interfaces, Nanotechnology 30 (2019) 025706, http://dx.doi.org/10.1088/1361-6528/aae874.
[24] C. Yi, X. Chen, F. Gou, C.M. Dmuchowski, A. Sharma, C. Park, C. Ke, Direct measurements of the mechanical strength of carbon nanotube - Aluminum interfaces, Carbon 125 (2017) 93–102, http://dx.doi.org/10.1016/j.carbon.2017.09.020.
[25] W. Zhou, G. Yamamoto, Y. Fan, H. Kwon, T. Hashida, A. Kawasaki, In-situ characterization of interfacial shear strength in multi-walled carbon nanotube reinforced aluminum matrix composites, Carbon 106 (2016) 37–47, http://dx.doi.org/10.1016/j.carbon.2016.05.015.
[26] A.V. Krasheninnikov, N. Berseneva, D.G. Kvashnin, J. Enkovaara, T. Björkman, P. Sorokin, D. Shtansky, R.M. Nieminen, D. Golberg, Toward stronger Al–BN nanotube composite materials: Insights into bonding at the Al/BN interface from first-principles calculations, J. Phys. Chem. C. 118 (2014) 26894–26901, http://dx.doi.org/10.1021/jp509505.
[27] D. Lahiri, V. Singh, L.H. Li, T. Xing, S. Seal, Y. Chen, A. Agarwal, Insight into reactions and interface between boron nitride nanotube and aluminum, J. Mater. Res. 27 (2012) 2760–2770, http://dx.doi.org/10.1557/jmr.2012.294.
[28] P.J. Eng, T.P. Trainor, G.E. Brown Jr., G.A. Waychunas, M. Newville, S.R. Sutton, M.L. Rivers, Structure of the hydrated α-Al2O3 (0001) surface, Science 288 (2000) 1029–1033, http://dx.doi.org/10.1126/science.288.5468.1029.
[29] G. Kresse, J. Furthmüller, Efficient iterative schemes for ab initio total-energy calculations using a plane-wave basis set, Phys. Rev. B . 54 (1996) 11169–11186.
[30] G. Kresse, D. Joubert, From ultrasoft pseudopotentials to the projector augmented-wave method, Phys. Rev. B. 59 (1999) 1758–1775, http://dx.doi.org/10.1103/PhysRevB.59.1758.
[31] G. Kresse, J. Hafner, Ab initio molecular dynamics for liquid metals, Phys. Rev. B. 47 (1993) 558–561, http://dx.doi.org/10.1103/physrevb.47.558.
[32] C. Rohmann, Q. Sun, D.J. Searles, Interaction of Al, Ti, and Cu atoms with boron nitride nanotubes: A computational investigation, J. Phys. Chem. C. 120 (2016) 3509–3518, http://dx.doi.org/10.1021/acs.jpcc.5b10698.
[33] P.A. Khomyakov, G. Giovannetti, P.C. Rusu, G. Brocks, J. van den Brink, P.J. Kelly, First-principles study of the interaction and charge transfer between graphene and metals, Phys. Rev. B. 79 (2009) 195425, http://dx.doi.org/10.1103/PhysRevB.79.195425.
[34] S. Gowtham, R.H. Scheicher, R. Ahuja, R. Pandey, S.P. Karna, Physisorption of nucleobases on graphene: Density-functional calculations, Phys. Rev. B. 76 (2007) 033401, http://dx.doi.org/10.1103/PhysRevB.76.033401.
[35] L. Radom, J.S. Binkley, J.A. Pople, The molecular structure of ammonia oxide (NH3O). An ab initio study, Aust. J. Chem. 30 (1977) 699–703, http://dx.doi.org/10.1071/ch9770699.
[36] W.H. Zachariasen, The crystal structure of monoclinic metaboric acid, Acta Crystallogr. 16 (1963) 385–389, http://dx.doi.org/10.1107/S0365110X6300102X.
[37] Z. Bai, L. Liu, D. Wang, C.-L. Hu, Z. Lin, To improve the key properties of nonlinear optical crystals assembled with tetrahedral functional building units, Chem. Sci. 12 (2021) 4014–4020, http://dx.doi.org/10.1039/D1SC00080B.
[38] S. Bagchi, C. Ke, H.B. Chew, Oxidation effect on the shear strength of graphene on aluminum and titanium surfaces, Phys. Rev. B. 98 (2018) 174106, http://dx.doi.org/10.1103/PhysRevB.98.174106.
[39] X. Lu, T. Dolmetsch, C. Zhang, Y. Chen, B. Boesl, A. Agarwal, In-situ synthesis of Boron Nitride Nanotube reinforced aluminum oxide composites by molecular mixing, Ceram. Int. 47 (2021) 13970–13979, http://dx.doi.org/10.1016/j.ceramint.2021.01.266.
[40] C. Yi, S. Bagchi, C.M. Dmuchowski, F. Gou, X. Chen, C. Park, H.B. Chew, C. Ke, Direct nanomechanical characterization of carbon nanotubes - titanium interfaces, Carbon 132 (2018) 548–555, http://dx.doi.org/10.1016/j.carbon.2018.02.069.
[41] C.M. Dmuchowski, C. Yi, F. Gou, A. Sharma, C. Park, C. Ke, Oxidation weakens interfaces in carbon nanotube reinforced titanium nanocomposites: An in situ electron microscopy nanomechanical study, Extreme Mech. Lett. 41 (2020) 101045, http://dx.doi.org/10.1016/j.eml.2020.101045.
[42] X. Chen, L. Zhang, M. Zheng, C. Park, X. Wang, C. Ke, Quantitative nanomechanical characterization of the van der waals interfaces between carbon nanotubes and epoxy, Carbon 82 (2015) 214–228, http://dx.doi.org/10.1016/j.carbon.2014.10.065.
[43] X. Chen, M. Zheng, C. Park, C. Ke, Direct measurements of the mechanical strength of carbon nanotube–poly(methyl methacrylate) interfaces, Small 9 (2013) 3345–3351, http://dx.doi.org/10.1002/smll.201202771.